nature chemical biology

ARTICLE

PUBLISHED ONLINE: 20 MARCH 2017 | DOI: 10.1038/NCHEMBIO.2335

The direct role of selenocysteine in [NiFeSe] hydrogenase maturation and catalysis

Marta C Marques[1], Cristina Tapia[2], Oscar Gutiérrez-Sanz[2], Ana Raquel Ramos[1], Kimberly L Keller[3,4,6], Judy D Wall[3,4], Antonio L De Lacey[2], Pedro M Matias[1,5]* & Inês A C Pereira[1]*

Hydrogenases are highly active enzymes for hydrogen production and oxidation. [NiFeSe] hydrogenases, in which selenocysteine is a ligand to the active site Ni, have high catalytic activity and a bias for H_2 production. In contrast to [NiFe] hydrogenases, they display reduced H_2 inhibition and are rapidly reactivated after contact with oxygen. Here we report an expression system for production of recombinant [NiFeSe] hydrogenase from *Desulfovibrio vulgaris* Hildenborough and study of a selenocysteine-to-cysteine variant (Sec489Cys) in which, for the first time, a [NiFeSe] hydrogenase was converted to a [NiFe] type. This modification led to severely reduced Ni incorporation, revealing the direct involvement of this residue in the maturation process. The Ni-depleted protein could be partly reconstituted to generate an enzyme showing much lower activity and inactive states characteristic of [NiFe] hydrogenases. The Ni-Sec489Cys variant shows that selenium has a crucial role in protection against oxidative damage and the high catalytic activities of the [NiFeSe] hydrogenases.

Hydrogenases catalyze the simplest of chemical reactions—the reversible conversion of protons and electrons to hydrogen. These metalloenzymes have attracted immense interest because they are extremely active catalysts for these reactions and can be applied in fuel cells, electrocatalytic or photocatalytic devices and serve as models for synthetic catalysts[1–4]. Of particular interest are systems aiming at artificial photosynthesis for solar-based H_2 production from water splitting, forming the basis for a carbon-free, hydrogen-fueled economy[5,6]. In terms of enzyme-based systems, [FeFe] hydrogenases are an obvious choice for this application, as they have the highest H_2 production activities[7,8], but these enzymes are irreversibly inactivated by even trace amounts of O_2, which limits their use in H_2 evolution devices. In contrast, [NiFe] hydrogenases can be reductively reactivated after exposure to O_2, but the standard enzymes form inactive Ni(III) species (Ni-A and Ni-B), of which Ni-A reactivates only very slowly[9]. A group of [NiFe] hydrogenases are O_2 tolerant[10], producing only the rapidly reactivated Ni-B species upon contact with O_2, but these enzymes are not suited for H_2 production owing to a very strong bias toward H_2 oxidation and pronounced H_2 inhibition of H^+ reduction[3].

The subfamily of [NiFeSe] hydrogenases[11], which have a selenocysteine as a direct ligand to the active site Ni (**Fig. 1a**,**b**), are the enzymes that display the most interesting properties for H_2 evolution applications[12]. They have a fast rate and catalytic bias toward H_2 production, in contrast to standard [NiFe] hydrogenases[13–15], and show much less product inhibition by H_2 (refs. 15–17). In addition, they do not form the inactive Ni(III) species characteristic of [NiFe] hydrogenases and are reactivated quickly at low potentials[16,18–21], being capable of H_2 production in the presence of small amounts of O_2 (refs. 15,16). These properties have been exploited in biocatalytic applications of [NiFeSe] hydrogenases for photo- and electrochemical H_2 production[14,17,22–26] and also for electrochemical ATP synthesis[27]. Furthermore, the superiority of [NiFeSe] hydrogenases has also been revealed *in vivo*, as these enzymes are preferentially expressed when selenium is available[28,29]. For example, in *D. vulgaris* Hildenborough the [FeFe] and [NiFe] hydrogenases are downregulated in the presence of selenium, indicating a physiological preference for the [NiFeSe] hydrogenase[29].

However, the incorporation of selenocysteine requires a complex dedicated machinery and has a very high energetic cost. Given also that sulfur is a much more abundant element than selenium, there must a strong biological advantage for using selenocysteine over cysteine[30,31]. Selenoproteins are mostly oxidoreductases in which selenocysteine is involved in the catalytic reaction. Despite numerous studies, there is still no consensus about why selenocysteine is used in selenoenzymes. The most studied group is that involved in thiol-disulfide exchange reactions, and possible factors discussed include selenocysteine's lower pK_a compared to cysteine, its increased nucleophilicity, increased electrophilicity, higher polarizability and hypervalency, better leaving group ability or a combination of all these, as selenocysteine performs multiple roles during the catalytic cycle[31,32]. However, several cysteine homologs of selenocysteine-containing enzymes can catalyze their enzymatic reactions with high catalytic efficiency, raising questions about the real necessity for selenium[32,33]. Another important argument for the superiority of selenocysteine is its ability to resist irreversible oxidative inactivation[31,33,34]. In fact, although selenium is more easily oxidized than sulfur, the resulting selenium oxides are much more electrophilic and unstable than their sulfur analogs and therefore easier to reduce back to the parent state. Thus, oxidation of the selenocysteine residue to the corresponding selenenic or seleninic acids is readily reversible, whereas reduction of a sulfenic acid is more difficult, and that of a sulfinic acid virtually impossible[34,35]. This property apparently enables selenoenzymes to better resist irreversible oxidative inactivation compared to their cysteine counterparts[34].

Here we report the first recombinant expression system for a [NiFeSe] hydrogenase allowing the production of engineered forms of the enzyme. We generated a protein variant in which the selenocysteine residue was replaced by cysteine, converting the [NiFeSe] enzyme into a [NiFe] hydrogenase and thus enabling us to

[1]Instituto de Tecnologia Química e Biológica António Xavier, Universidade Nova de Lisboa, Oeiras, Portugal. [2]Instituto de Catálisis y Petroleoquímica (CSIC), Madrid, Spain. [3]Biochemistry Department, University of Missouri, Columbia, Missouri, USA. [4]Ecosystems and Networks Integrated with Genes and Molecular Assemblies (ENIGMA), Berkeley, California, USA. [5]Instituto de Biologia Experimental e Tecnológica (iBET), Oeiras, Portugal. [6]Present address: Biology Department, William Woods University, Fulton, Missouri, USA. *e-mail: ipereira@itqb.unl.pt or matias@itqb.unl.pt

distinguish the effect of the selenocysteine residue from that of the protein structure in the catalytic properties and oxygen tolerance of these enzymes. This single mutation had a high impact on the active site, strongly affecting nickel incorporation, catalytic activity and O_2 sensitivity of the resulting enzyme.

RESULTS

The recombinant *D. vulgaris* [NiFeSe] hydrogenase

To set up an expression system for a [NiFeSe] hydrogenase, we opted for homologous expression of the enzyme in *D. vulgaris* Hildenborough, given the known specificity of the maturation proteins and the selenocysteine insertion machinery. The native *D. vulgaris* [NiFeSe] hydrogenase (comprised of HysA and HysB) is a lipoprotein bound to the membrane by a lipidic group linked to Cys4 of the large subunit HysA[36]. We designed an expression vector for a soluble form of this hydrogenase in which the first 11 residues of HysA, containing the lipobox that directs attachment of the lipid group, were removed. Such a soluble form is also produced by native *D. vulgaris* cells[13]. This vector was used to transform *D. vulgaris* Hildenborough by electroporation, generating a strain that expresses a soluble periplasmic form of the enzyme (**Supplementary Results**, **Supplementary Fig. 1**). The recombinant [NiFeSe] (r[NiFeSe]) hydrogenase was purified by affinity chromatography based on a *Strep*-tag fused to the N terminus of HysA. The purified r[NiFeSe] hydrogenase displayed a H_2 production activity of 8,280 ± 382 s^{-1} (5,640 ± 260 U mg^{-1}) (**Table 1**), which is close to the maximal activity reported for the native wild-type (WT) enzyme in the presence of phospholipids (10,134 s^{-1} (6,908 U mg^{-1})), and much higher than the value previously reported for the soluble form (847 s^{-1} (580 U mg^{-1}))[13].

To confirm the structural integrity of the r[NiFeSe] hydrogenase, we purified and crystallized it anaerobically. The structure, refined to 0.95-Å resolution, revealed the recombinant enzyme to be identical to the WT form without presenting any oxidative damage. Thus, the expression system was successful in producing fully active enzyme in a native configuration. The active site (**Fig. 1c**) was found in a conformation that corresponds to the reduced state (Sec489 in conformer III)[20,37], as reported for the reduced enzyme from *Desulfomicrobium* (*Dm.*) *baculatum*[38]. Two Ni positions (referred to as Ni-1 and Ni-2) were observed ~1 Å from each other, both bound to Sec489, and the total Ni occupancy was only 87%. The selenocysteine residue had three slightly different positions, corresponding to binding of Ni-1 (81%), Ni-2 (7%) and no Ni (12%). The identification of the minor Ni site (Ni-2) was possible only with the near atomic resolution of the diffraction data. The Ni–Se bond distances were similar for both sites (2.31 Å and 2.25 Å, respectively) and the Ni–Fe distance changed from 2.55 Å (Ni-1) to 3.17 Å (Ni-2). These active site features were initially inferred from $2|F_o| - |F_c|$ and $|F_o| - |F_c|$ maps (**Supplementary Fig. 2a**) and then confirmed from the calculated anomalous difference maps (**Supplementary Fig. 2b**). Different Ni positions were also identified in the crystal structures of oxidized *Dm. baculatum* [NiFeSe] hydrogenase[39].

We also isolated and crystallized the r[NiFeSe] hydrogenase under aerobic conditions and refined the resulting structure (r[NiFeSe]-Ox) to 1.30-Å resolution. Previous structures of aerobically crystallized [NiFeSe] hydrogenases show oxidative modifications in the active site[20,39], which are due to O_2 exposure during purification and especially the long crystallization periods. In the case of r[NiFeSe]-Ox, the active site was present in three different conformations (**Supplementary Fig. 3a–e**) owing to the presence of an exogenous sulfur bound to Ni, as previously described[20]. There was also evidence for oxidative damage, as Cys75, one of the terminal ligands to Ni, was oxidized to sulfenate (36%) and sulfinate (64%), whereas in previous structures[20,37] it was fully oxidized to sulfinate. Also, the proximal [4Fe-4S] cluster suffered partial oxidative damage (~24%) to a form that was refined as [4Fe-4S-2O] (**Supplementary Fig. 3f–h**). The total Ni occupancy of the active site refined to 85%, and a minor Ni site could not be clearly identified in this structure.

According to experimental data[40] and molecular dynamics simulations[41] of [NiFe] hydrogenases, the most probable proton transfer pathway in both [NiFe] and [NiFeSe] hydrogenases involves a glutamate residue (Glu28 in the *D. vulgaris* enzyme) that receives protons from the active site. The refined r[NiFeSe] structure suggested a possible interaction between Sec489 and the carboxyl group of Glu28, in which the distance between the selenium atom and the $O^{\varepsilon 1}$ of Glu28 is ~3.3 Å. This value is in the range expected for a hydrogen bond, hinting at H^+ transfer between Sec489 and Glu28.

The impact of the Sec489Cys substitution

We constructed Sec489Cys hydrogenase, a variant [NiFeSe] hydrogenase in which the selenocysteine residue is exchanged for a cysteine, converting it to a [NiFe] enzyme. The H_2 production activity

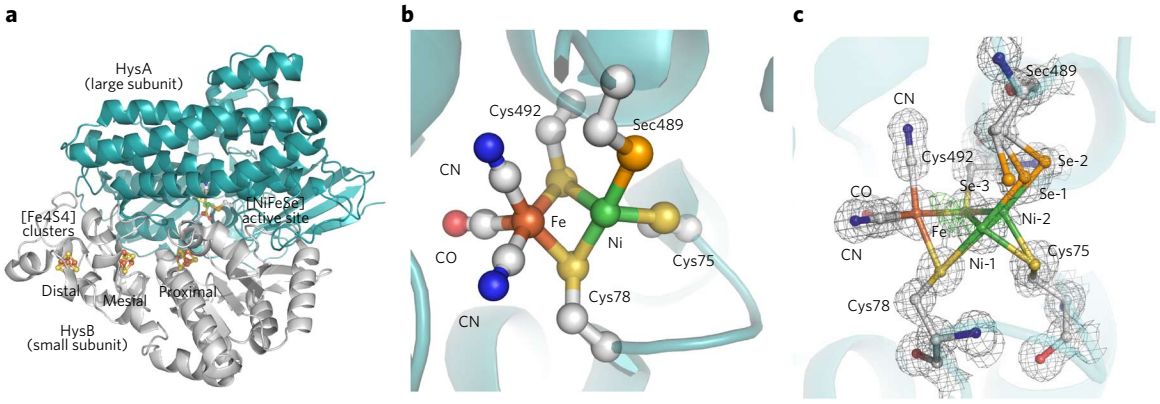

Figure 1 | The 3D structure of *D. vulgaris* [NiFeSe] hydrogenase. (**a**,**b**) Overall (**a**) and detailed (**b**) views of the reduced structure of the native soluble protein after aerobic purification and crystallization (PDB 3ZE7). In **a**, the two protein chains are displayed as cartoons; the [NiFeSe] active site, its coordinating ligands and the three [Fe4S4] clusters are shown in ball-and-stick representation. In **b**, the [NiFe] binuclear center and the side chains of its coordinating protein ligands are shown as a ball-and-stick model, and the HysA protein chain as a semitransparent cartoon. The oxidative damage of Cys75 was omitted. (**c**) The [NiFeSe] active site and its surroundings in the crystal structure of the anaerobically purified and crystallized r[NiFeSe] hydrogenase and its corresponding $2|F_o| - |F_c|$ (gray mesh, 1.5 map r.m.s.) and $|F_o| - |F_c|$ (green mesh, 3.5 map r.m.s.) maps. No negative peaks are visible at –3.5 r.m.s. in the $|F_o| - |F_c|$ map. Atoms are color coded as follows: brown, Fe; green, Ni; gold, S; red, O; gray, C; blue, N; orange, Se. H atoms omitted for clarity.

Table 1 | Enzymatic activity of the different *D. vulgaris* [NiFeSe] hydrogenase variants

	Turnover rate (s^{-1})			
	$[NiFeSe]_m$ hydrogenase[a]	r[NiFeSe] hydrogenase	Ni-depleted Sec489Cys hydrogenase	Ni-Sec489Cys hydrogenase
Ni content[b]	~99%[c]	~85%	~15%	~60%
H_2 production	10,134	8,280 ± 382	6.6 ± 2.6	183 ± 10
H_2 uptake	1,320	2,430 ± 175	N.D.	85 ± 13
	Isotopic D_2–H^+ exchange activity			
HD + H_2 evolution	N.D.	2,000 ± 300	N.D.	66 ± 7

[a]Reported activity of the native, membrane-associated [NiFeSe] hydrogenase[13]. [b]As determined from the crystal structures. [c]Value determined from a refined crystal structure of native soluble enzyme. N.D., not determined. Values represent mean of at least 3 independent experiments ± s.d. (see text and Online Methods).

of the isolated Sec489Cys hydrogenase was drastically reduced, to 4.5 ± 1.8 U mg^{-1}, which corresponded to a turnover rate of 6.6 ± 2.6 s^{-1} (0.08% of the r[NiFeSe] activity). Nevertheless, the CD spectrum of the Sec489Cys variant was identical to that of the r[NiFeSe] protein, indicating that it was properly folded (**Supplementary Fig. 4**). The structure of the aerobically crystallized Sec489Cys hydrogenase was refined to a resolution of 1.4 Å. Surprisingly, the structure revealed that most of the protein molecules lacked Ni at the active site (only ~15% Ni occupancy). Instead, a putative sulfur species (85% occupancy) was found in place of the missing Ni atom (**Fig. 2a–c**). The sulfur ligand completed the octahedral coordination of the Fe atom (2.4 Å) and could also be covalently bound to Cys489 S^{γ} (at 2.1 Å). This residue, which corresponds to selenocysteine in the WT protein, was partly oxidized to sulfenate (C^{β}-$S^{\gamma}O$, 18%) and sulfinate (C^{β}-$S^{\gamma}O_2$, 63%) as assessed from the refined occupation factors of the oxygen atoms. The near absence of Ni resulted in the presence of three different conformations for the Ni ligand Cys75. In the first conformation (32%) the Cys75 was oxidized to sulfenate and coordinating the Ni atom (**Fig. 2b**), whereas the other two conformations (37% and 31%) were observed when Ni was absent and suggested a disulfide bond between Cys75 and Cys78 (**Fig. 2c**). The proximal [4Fe-4S] cluster was 26% oxygen damaged to [4Fe-4S-2O].

Reconstitution of the Ni–Fe active site

In an attempt to increase the Ni content of the Sec489Cys hydrogenase, cells were first grown with increasing Ni concentrations (up to 200 μM), as it was previously shown that deletion of the genes encoding HypA and HypB, the proteins responsible for Ni insertion[42,43], could be overcome by growth in the presence of high Ni concentrations[42]. However, no meaningful effect was achieved by this approach. Next, we tested several conditions for *in vitro* reconstitution of the active site of the Sec489Cys hydrogenase and obtained the best results by adding $NiCl_2$ to the cell disruption buffer and incubating the purified enzyme with $NiCl_2$ under H_2 (**Supplementary Fig. 5**). The H_2 production activity of the reconstituted enzyme (Ni-Sec489Cys hydrogenase) increased with increasing concentrations of Ni, up to a value of 183 ± 10 s^{-1} (125 ± 7 U mg^{-1}). This activity is comparable to that observed for the native *D. vulgaris* $[NiFe]_1$ hydrogenase (287 s^{-1}, 174 U mg^{-1})[13], indicating substantial Ni integration into the active site. Quantification of Ni versus Fe content by inductively coupled plasma atomic emission spectroscopy consistently indicated an excess of bound Ni in the reconstituted enzyme (11 ± 1 Fe/Ni in Sec489Cys versus 15 ± 1 Fe/Ni in WT) (**Supplementary Table 1**). Thus, the *in vitro* reconstitution protocol leads to Ni incorporation into the active site but also to some unspecific Ni binding to the protein.

Notably, the H_2 uptake activity of the Ni-Sec489Cys hydrogenase (85 ± 13 s^{-1}) was closer to its H_2 production activity than for the r[NiFeSe] hydrogenase, indicating a stronger effect of the Sec489Cys substitution on the H_2 production than on the H_2 uptake activity (**Table 1**). We measured the pH profiles of both activities for the r[NiFeSe] and Ni-Sec489Cys hydrogenases. The profiles were quite similar, with optimum pH values close to 6.0 for H_2 production and near 11 for H_2 uptake, in agreement with the values reported for the WT [NiFeSe] hydrogenase[44]. The pH profile of the H–D exchange activity was also measured for the r[NiFeSe] and Ni-Sec489Cys hydrogenases (**Supplementary Fig. 6**). The profiles were again very similar, with the same optimum pH value at 6.0, although the maximum exchange activity measured for the Ni-Sec489Cys hydrogenase (66 ± 7 s^{-1}) was approximately 15 times smaller than that of the r[NiFeSe] hydrogenase.

Structures of the Ni-Sec489Cys hydrogenase

The Ni-reconstituted Sec489Cys enzyme was purified and crystallized both anaerobically (Ni-Sec489Cys) and aerobically (Ni-Sec489Cys-Ox). In the anaerobic protocol there was a brief contact with oxygen during concentration of the protein that was performed aerobically. This is a quick procedure and in the recombinant enzyme did not lead to any oxidative damage. In contrast, in both crystal structures of the Ni-Sec489Cys enzyme the electron density at the active site revealed a similar complex mixture of oxidized states: Cys489 (selenocysteine in the WT protein) was partially oxidized to sulfinate, and Cys75 was partly oxidized to sulfenate. In contrast, in the anaerobically purified and crystallized r[NiFeSe] hydrogenase prepared using the same procedure (including aerobic protein concentration), no oxidative damage was observed for these two residues.

The anaerobic Ni-Sec489Cys crystal structure at 1.04-Å resolution confirmed substantial Ni incorporation into the active site, with a total Ni occupancy refined to 61% (**Fig. 3a**). This incorporation level allowed a comparison between the Ni-Sec489Cys hydrogenase and standard [NiFe] hydrogenases. Considering the measured activity of 183 ± 1 s^{-1} and a Ni content of ~60%, the maximal H_2 production activity of the fully Ni-loaded Sec489Cys hydrogenase would be around 300 s^{-1}, which is comparable to the values reported for [NiFe] hydrogenases, and <4% of the value measured for the r[NiFeSe] enzyme (**Table 1**). An anomalous difference map (**Supplementary Fig. 7**) combined with the near-atomic data resolution allowed the identification of three different positions for the Ni atom in the active site. Two of them corresponded to the Ni-1 and Ni-2 sites described for the r[NiFeSe] structure (**Fig. 3b**,**c**). The third Ni site was ~1 Å away from the other two but did not match a standard active site geometry, suggesting it was a transient species formed during reconstitution. Its low refined occupancy (6%) obscured the coordination details. Cys489 (selenocysteine in the WT protein) was 59% oxidized to sulfinate, and four different conformations for Cys75 were observed. Two of them corresponded to the coordination of the Ni-1 and Ni-2 sites (**Fig. 3b**,**c**), and the other two were observed in the absence of Ni and suggested a disulfide bond between Cys75 and Cys78 (**Fig. 3d**). A partly occupied exogenous sulfur was found at the active site, occupying the Ni position as

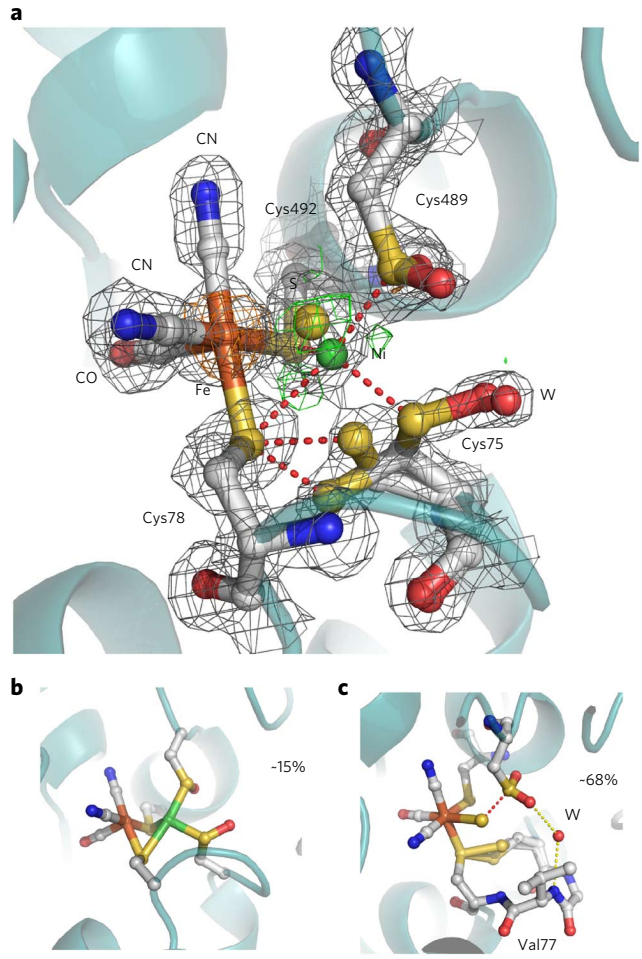

Figure 2 | The active site and its surroundings in the crystal structure of Sec489Cys-Ox. (**a**) The refined structure superimposed with corresponding $2|F_o| - |F_c|$, $|F_o| - |F_c|$ maps (as in **Fig. 1c**) and anomalous Fourier maps (orange mesh, 4.5 map r.m.s.). Red dashed lines represent presumed chemical bonds. (**b**,**c**) Probable predominant structural forms of the active site, and their relative percentages, as interpreted from the final refined structure (Online Methods). (**b**) The Ni-containing minor component, with Ni bound to Cys489 and Cys75 sulfenates. (**c**) The Ni-depleted major component, with an exogenous S atom completing the octahedral coordination of the Fe and possibly bound to Cys489 (red dashed line). Cys75 in two conformations forms a disulfide bond with Cys78. A water molecule is hydrogen bonded (yellow dashed lines) to an O from the Cys489 sulfinate and the peptide hydrogen H from Val77. Atom color scheme and representations are as in **Figure 1**. H atoms were omitted for clarity.

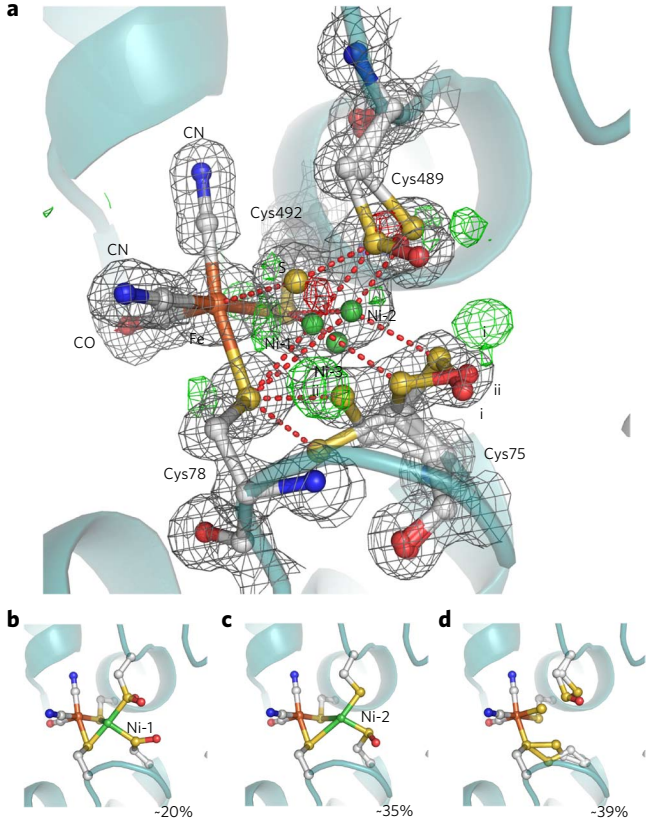

Figure 3 | The active site and its surroundings in the crystal structure of the anaerobically purified and crystallized Ni-Sec489Cys hydrogenase. (**a**) The final refined structure with $2|F_o| - |F_c|$ and $|F_o| - |F_c|$ maps (as in **Fig. 1c**), showing the three Ni positions and the conformations of Cys75 and Cys489. The positive peaks ((i) and (ii)) in the final $|F_o| - |F_c|$ map probably correspond to the similarly labeled terminal O atoms of the sulfinate forms of Cys75 in further side chain orientations (not modeled). Red dashed lines represent presumed chemical bonds. (**b**–**d**) The predominant structural forms of the active site, and their relative percentages, as interpreted from the final refined structure. (**b**) The Ni-1 site bound to Cys489 in its sulfinate form and Cys75 in one of its sulfenate forms. (**c**) The Ni-2 site bound to Cys489 and Cys75 in the second sulfenate form. (**d**) The Ni-depleted form, with Cys75 forming a disulfide bond with Cys78, Cys489 probably as a mixture of cysteine and sulfinate and an exogenous S atom completing the octahedral coordination of the Fe atom. Atom colors and HysA protein chain are as in **Figure 1**. H atoms omitted for clarity.

observed in the structure of the nonreconstituted Sec489Cys variant (**Fig. 3d**). Notably, despite the substantial oxygen damage at the active site, the proximal [4Fe-4S] cluster was found in the canonical cubane form, in agreement with the very short oxygen exposure.

In the aerobic Ni-Sec489Cys-Ox crystal structure at 1.35 Å resolution, the Ni occupancy refined to 44% (**Supplementary Fig. 8**). This lower Ni occupancy at the active site was due to the fact that the second Ni position was not modeled owing to the lower data resolution. However, the electron density suggested it was present ~0.9 Å from the first Ni, as in the r[NiFeSe] and Ni-Sec489Cys structures. Cys489 was 75% oxidized to sulfinate, and the same four conformations for Cys75 were observed as with the Ni-Sec489Cys structure. Most notably, unlike the previous structures, a bridging oxy ligand refined as OH^- (61%) was present between Ni and Fe, similarly to the bridging oxide ligand in the crystal structures of oxidized [NiFe] hydrogenases. In this structure, the proximal [4Fe-4S] cluster was 33% oxygen damaged to [4Fe-4S-2O].

Spectroscopic evidence for a typical [NiFe] active site

In the as-isolated oxidized form of the native WT [NiFeSe] hydrogenase, the FTIR spectrum showed the active site to be present in two different conformations, termed Ni-IS_I and Ni-IS_{II}, where the first conformation corresponded to the more intense CO band at 1,904 cm^{-1} and the second to a CO band at 1,939 cm^{-1} (ref. 19). We also analyzed the aerobically isolated r[NiFeSe] hydrogenase by FTIR (**Fig. 4a**) and found that it was more than 80% in the Ni-IS_{II} state, as deduced from the intense CO band at 1,940 cm^{-1} and CN^- bands at 2,079 and 2,094 cm^{-1}. This indicated a higher homogeneity of the active site in the recombinant enzyme. Nevertheless, upon reduction with H_2, the r[NiFeSe] hydrogenase displayed a mixture of two Ni-R isoforms (CO bands at 1,910 and 1,935 cm^{-1} and several

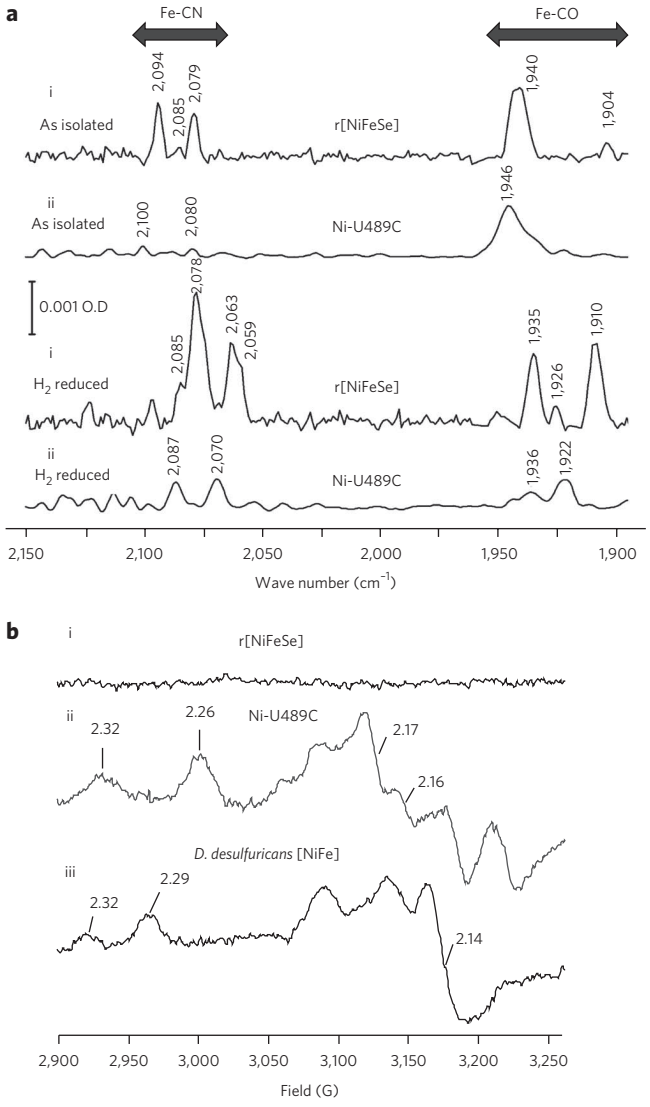

Figure 4 | Spectroscopic characterization of the Ni-Sec489Cys variant versus the r[NiFeSe] hydrogenase. (**a**,**b**) FTIR (**a**) and EPR (**b**) spectra of the r[NiFeSe] hydrogenase purified aerobically (**a**, i and **b**, i), Ni-Sec489Cys variant purified anaerobically and then exposed to air (**a**, ii and **b**, ii) and *Desulfovibrio desulfuricans* [NiFe] hydrogenase purified under air (**b**, iii) (shown for comparison).

overlapping CN^- bands in the range of 2,059–2,085 cm^{-1}). The presence of these two forms revealed structural heterogeneity that could be related to the observation of two Ni positions in the structure of the reduced state (r[NiFeSe]).

In the FTIR spectra of the Ni-Sec489Cys hydrogenase (**Fig. 4a**), the active site bands were similar to those of standard O_2-sensitive [NiFe] hydrogenases, both in the oxidized and in the reduced state[9]. In particular, the overlapping bands around 1,946 cm^{-1} due to the CO stretching vibration in the oxidized state resembled the Ni-A and Ni-B FTIR spectra of standard [NiFe] hydrogenases. Therefore, the FTIR spectra also indicated that the electron density distribution in the active site of the Ni-Sec489Cys hydrogenase resembled that of a [NiFe] hydrogenase.

The [NiFeSe] hydrogenases do not form the Ni-A or Ni-B inactive states typical of [NiFe] hydrogenases, and are EPR silent in the oxidized state[18]. The EPR spectrum of the aerobic Ni-Sec489Cys hydrogenase (**Fig. 4b**) showed signals indicating the presence of both Ni-A and Ni-B species (g_{max} = 2.32 and 2.26). In contrast, the r[NiFeSe] enzyme was EPR silent in the same conditions (**Fig. 4b**), as previously described.

DISCUSSION

Selenocysteine-containing enzymes were initially believed to be restricted to anaerobes, given the ease of oxidation of the selenocysteine residue, which could make it unsuitable for aerobic conditions[45]. However, evolutionary studies of selenoproteins have instead indicated that their numbers have gone up after increases in oxygen levels in the atmosphere, suggesting that selenocysteine is helpful in adaptation to an aerobic environment[33,46]. Selenocysteine is also present in many enzymes involved in antioxidant defense, which may seem paradoxical, as selenium is more easily oxidized than sulfur. This is apparently related to the fact that selenium reacts with O_2 and reactive oxygen species in a very reversible manner, as selenium oxides are much easier to reduce than sulfur oxides.

The process of oxidative inactivation is of particular importance for the development of biotechnological applications of hydrogenases, which include the [NiFeSe] hydrogenases, a group of selenoenzymes. However, the role of selenocysteine in catalysis versus oxygen tolerance has not been directly investigated in this family of enzymes. In the [NiFeSe] hydrogenases, the selenocysteine residue is believed to be directly involved in catalysis, and the corresponding cysteine residue in the [NiFe] enzymes has been shown to bind a H^+ resulting from H_2 oxidation, in the most reduced state (Ni-R)[47].

We developed an expression system for the *D. vulgaris* Hildenborough [NiFeSe] hydrogenase that enables the production of variant forms of the enzyme. The availability of a system to produce recombinant [NiFeSe] hydrogenase provides a ready supply of the enzyme for future detailed studies and enables enzyme engineering to generate variants with improved properties. The recombinant enzyme was produced in a soluble form, which greatly facilitates further studies and applications. It showed high catalytic activity, comparable to the native enzyme, and was structurally identical. The recombinant enzyme showed slightly less than full Ni incorporation into the active site (~90%), suggesting that the native maturation machinery responsible for Ni insertion could not keep up with the rate of protein expression. Two crystal structures at near-atomic resolution, obtained in anaerobic and aerobic conditions, revealed that Ni can be present in more than one position, as recently reported for the [NiFeSe] enzyme from *Dm. baculatum*[39], and allowed the reassignment of the oxygen-damaged form of the proximal cluster as [4Fe-4S-2O]. The presence of Ni positions with different Ni–Fe distances is conspicuous and raises the question of whether some of these positions could correspond to inactive states of the enzyme. Further studies are required to address this point. The aerobically crystallized enzyme showed less oxidative damage than previously reported[20,37], probably owing to the faster affinity purification protocol. In the case of *Dm. baculatum*, the enzyme purified aerobically was present in a very complex mixture of oxidized states[39], and the protein had to be purified anaerobically to obtain better resolved structures. Still, a heterogeneous active site with a mixture of states was also observed for the protein crystallized under air. An important difference from the *D. vulgaris* r[NiFeSe] hydrogenase was that the selenocysteine was oxidized to a mixture of selenenate and seleninate, which were not observed in the *D. vulgaris* enzyme. Instead, oxidation to a sulfinate was observed at the Ni-terminal ligand Cys75, which is an irreversible change. The absence of selenium oxides in the *D. vulgaris* enzyme may be related to the presence of the exogenous sulfur atom at the active site, which induces side chain conformations of selenocysteine (conformers I and II) not found in the equivalent cysteine residue in [NiFe] hydrogenases (always conformer III), that limits access to the selenium atom[20]. Alternatively, such selenium oxides may be formed only transiently, in contrast to the sulfinate modification of Cys75.

The high heterogeneity in the active site of the oxidized [NiFeSe] hydrogenases, as revealed by FTIR[15,19,39], is in agreement with a facile production of selenium oxides, which can be rapidly reduced when the enzyme is reactivated[16,19,21]. Nevertheless, the overall structure of the NiFe active site in the Sec489Cys variant was very similar to those in other standard [NiFe] hydrogenases, aside from some local differences in the surroundings that are due to differences in amino acid sequences (**Supplementary Fig. 9**).

The structure of the Sec489Cys variant revealed that Ni incorporation was dramatically compromised by the selenocysteine-to-cysteine substitution. This finding reveals the direct involvement of this active site residue in the Ni incorporation process. The insertion of Ni into the active site involves the HypA and HypB proteins and occurs only after insertion of the $Fe(CN)_2CO$ moiety[42]. However, how the HypA and HypB proteins interact with the hydrogenase large subunit has not been elucidated. Our results indicate that Sec489 is directly involved in the incorporation process, possibly acting as a nucleophile to attack the Ni atom bound to HypA and/or HypB. The drastically reduced Ni content of the Sec489Cys hydrogenase suggests that the lower nucleophilicity of the cysteine residue in this variant compromises this process. In *D. vulgaris*, there are two HypA (DVU2292 and DVU2328) and one HypB (DVU2329) homologs, for the maturation of four [NiFe] and one [NiFeSe] hydrogenases. This suggests that at least one HypA protein will be involved in the maturation of multiple enzymes. If the same HypA protein is responsible for Ni insertion in the [NiFeSe] and one or more of the [NiFe] enzymes, one would not expect that the Sec489Cys substitution would affect Ni incorporation, unless, in the case of the [NiFe] hydrogenase homolog(s), the nucleophilicity of the Ni-coordinating cysteine residue is enhanced by nearby residues before the protein is fully folded, which would not be required in the case of the [NiFeSe] enzyme owing to the intrinsic higher nucleophilicity of selenium. Alternatively, an unknown protein other than HypA may be involved in the maturation of the [NiFeSe] enzyme. Further work will be required to elucidate this key point.

Notably, incubation of the isolated Sec489Cys hydrogenase with Ni enabled further incorporation of this metal, allowing a comparison of the reconstituted variant with standard [NiFe] hydrogenases. To our knowledge, this is the first report of *in vitro* Ni reconstitution of an isolated [NiFe] hydrogenase, opening new possibilities for investigation of the active site maturation. We observed a third Ni site in the Ni-Sec489Cys structure, suggesting it corresponds to a trapped intermediate of the *in vitro* insertion of Ni into the active site. The fully reconstituted Ni-Sec489Cys hydrogenase had at best 4% of the H_2-production activity of the recombinant r[NiFeSe] enzyme, which is a direct result of the lower chemical reactivity of cysteine versus selenocysteine. The [NiFeSe] hydrogenases display a bias toward H_2 production, in contrast to the [NiFe] enzymes. In the Ni-Sec489Cys variant, the H_2 production activity was more strongly reduced than the H_2 oxidation one, which agrees with the fact that selenocysteine is more acidic than cysteine, and thus favors H_2 production. Interestingly, the optimal pH for both H_2 production/oxidation and H–D exchange activities was similar for the r[NiFeSe] and Ni-Sec489Cys proteins, indicating that this residue does not have a major role in determining the pH optimum for both activities.

The structures of the Ni-Sec489Cys hydrogenase revealed that this substitution has a dramatic effect on the oxygen sensitivity of the active site. Oxidative damage was present even in the anaerobically purified and crystallized enzyme, which was not observed in the r[NiFeSe] form treated in exactly the same conditions. The oxidative modification was even present in Cys489, even though a sulfur ligand was also present at the active site, which in the r[NiFeSe] form is presumed to protect the corresponding Sec489 residue from contact with O_2. Furthermore, the structural evidence indicated that in the oxidized structure (Ni-Sec489Cys-Ox) a bridging oxy species, presumably OH^-, was present at the active site, as in the inactive oxidized forms of [NiFe] hydrogenases. The FTIR and EPR characterization of the Ni-Sec489Cys hydrogenase also agreed with the presence of inactive Ni-A and Ni-B species, associated with the presence of bridging oxide species. However, and in contrast with the oxidized structure of the r[NiFeSe] enzyme (r[NiFeSe]-Ox), the Cys75 Ni ligand was not oxidized to sulfinate. This observation suggests that the oxidation of Cys489 changes the electron distribution at the active site, diminishing the reactivity of Cys75 toward oxygen. Our results strongly suggest that selenocysteine is directly responsible for the increased oxygen tolerance and rapid recovery from oxygen damage of [NiFeSe] hydrogenases, as well as for their higher catalytic efficiency, particularly for H_2 production. Furthermore, this study revealed that the selenocysteine/cysteine ligand is directly involved in Ni incorporation, providing further insight into the maturation process of [NiFe] and [NiFeSe] hydrogenases.

Received 7 June 2016; accepted 21 December 2016;
published online 20 March 2017

METHODS

Methods, including statements of data availability and any associated accession codes and references, are available in the online version of the paper.

References

1. Vincent, K.A., Parkin, A. & Armstrong, F.A. Investigating and exploiting the electrocatalytic properties of hydrogenases. *Chem. Rev.* **107**, 4366–4413 (2007).
2. King, P.W. Designing interfaces of hydrogenase-nanomaterial hybrids for efficient solar conversion. *Biochim. Biophys. Acta* **1827**, 949–957 (2013).
3. Lubitz, W., Ogata, H., Rüdiger, O. & Reijerse, E. Hydrogenases. *Chem. Rev.* **114**, 4081–4148 (2014).
4. Simmons, T.R., Berggren, G., Bacchi, M., Fontecave, M. & Artero, V. Mimicking hydrogenases: From biomimetics to artificial enzymes. *Coord. Chem. Rev.* **270–271**, 127–150 (2014).
5. Friedrich, B., Fritsch, J. & Lenz, O. Oxygen-tolerant hydrogenases in hydrogen-based technologies. *Curr. Opin. Biotechnol.* **22**, 358–364 (2011).
6. Wakerley, D.W. & Reisner, E. Oxygen-tolerant proton reduction catalysis: much O_2 about nothing? *Energy Environ. Sci.* **8**, 2283–2295 (2015).
7. Brown, K.A., Wilker, M.B., Boehm, M., Dukovic, G. & King, P.W. Characterization of photochemical processes for H_2 production by CdS nanorod-[FeFe] hydrogenase complexes. *J. Am. Chem. Soc.* **134**, 5627–5636 (2012).
8. Hambourger, M. *et al.* [FeFe]-hydrogenase-catalyzed H_2 production in a photoelectrochemical biofuel cell. *J. Am. Chem. Soc.* **130**, 2015–2022 (2008).
9. De Lacey, A.L., Fernandez, V.M., Rousset, M. & Cammack, R. Activation and inactivation of hydrogenase function and the catalytic cycle: spectroelectrochemical studies. *Chem. Rev.* **107**, 4304–4330 (2007).
10. Fritsch, J., Lenz, O. & Friedrich, B. Structure, function and biosynthesis of O-tolerant hydrogenases. *Nat. Rev. Microbiol.* **11**, 106–114 (2013).
11. Baltazar, C.S.A. *et al.* Nickel–iron–selenium hydrogenases—an overview. *Int. J. Inorg. Chem.* **2011**, 948–962 (2011).
12. Wombwell, C., Caputo, C.A. & Reisner, E. [NiFeSe]-hydrogenase chemistry. *Acc. Chem. Res.* **48**, 2858–2865 (2015).
13. Valente, F.M.A. *et al.* Hydrogenases in *Desulfovibrio vulgaris* Hildenborough: structural and physiologic characterisation of the membrane-bound [NiFeSe] hydrogenase. *J. Biol. Inorg. Chem.* **10**, 667–682 (2005).
14. Rüdiger, O. *et al.* Enzymatic anodes for hydrogen fuel cells based on covalent attachment of Ni-Fe hydrogenases and direct electron transfer to SAM-modified gold electrodes. *Electroanalysis* **22**, 776–783 (2010).
15. Riethausen, J., Rüdiger, O., Gärtner, W., Lubitz, W. & Shafaat, H.S. Spectroscopic and electrochemical characterization of the [NiFeSe] hydrogenase from *Desulfovibrio vulgaris* Miyazaki F: reversible redox behavior and interactions between electron transfer centers. *ChemBioChem* **14**, 1714–1719 (2013).
16. Parkin, A., Goldet, G., Cavazza, C., Fontecilla-Camps, J.C. & Armstrong, F.A. The difference a Se makes? Oxygen-tolerant hydrogen production by the [NiFeSe]-hydrogenase from *Desulfomicrobium baculatum*. *J. Am. Chem. Soc.* **130**, 13410–13416 (2008).
17. Reisner, E., Fontecilla-Camps, J.C. & Armstrong, F.A. Catalytic electrochemistry of a [NiFeSe]-hydrogenase on TiO_2 and demonstration of its suitability for visible-light driven H_2 production. *Chem. Commun. (Camb.)* **5**, 550–552 (2009).

18. Teixeira, M. *et al.* Nickel-[iron-sulfur]-selenium-containing hydrogenases from *Desulfovibrio baculatus* (DSM 1743). Redox centers and catalytic properties. *Eur. J. Biochem.* **167**, 47–58 (1987).
19. De Lacey, A.L., Gutiérrez-Sánchez, C., Fernández, V.M., Pacheco, I. & Pereira, I.A.C. FTIR spectroelectrochemical characterization of the Ni-Fe-Se hydrogenase from *Desulfovibrio vulgaris* Hildenborough. *J. Biol. Inorg. Chem.* **13**, 1315–1320 (2008).
20. Marques, M.C., Coelho, R., De Lacey, A.L., Pereira, I.A. & Matias, P.M. The three-dimensional structure of [NiFeSe] hydrogenase from *Desulfovibrio vulgaris* Hildenborough: a hydrogenase without a bridging ligand in the active site in its oxidised, "as-isolated" state. *J. Mol. Biol.* **396**, 893–907 (2010).
21. Ceccaldi, P., Marques, M.C., Fourmond, V., Pereira, I.C. & Léger, C. Oxidative inactivation of NiFeSe hydrogenase. *Chem. Commun. (Camb.)* **51**, 14223–14226 (2015).
22. Reisner, E., Powell, D.J., Cavazza, C., Fontecilla-Camps, J.C. & Armstrong, F.A. Visible light-driven H(2) production by hydrogenases attached to dye-sensitized TiO(2) nanoparticles. *J. Am. Chem. Soc.* **131**, 18457–18466 (2009).
23. Caputo, C.A. *et al.* Photocatalytic hydrogen production using polymeric carbon nitride with a hydrogenase and a bioinspired synthetic Ni catalyst. *Angew. Chem. Int. Ed. Engl.* **53**, 11538–11542 (2014).
24. Sakai, T., Mersch, D. & Reisner, E. Photocatalytic hydrogen evolution with a hydrogenase in a mediator-free system under high levels of oxygen. *Angew. Chem. Int. Ed. Engl.* **52**, 12313–12316 (2013).
25. Caputo, C.A., Wang, L.D., Beranek, R. & Reisner, E. Carbon nitride-TiO2 hybrid modified with hydrogenase for visible light driven hydrogen production. *Chem. Sci.* **6**, 5690–5694 (2015).
26. Mersch, D. *et al.* Wiring of photosystem II to hydrogenase for photoelectrochemical water splitting. *J. Am. Chem. Soc.* **137**, 8541–8549 (2015).
27. Gutiérrez-Sanz, Ó. *et al.* H2-fueled ATP synthesis on an electrode: mimicking cellular respiration. *Angew. Chem. Int. Ed. Engl.* **55**, 6216–6220 (2016).
28. Berghöfer, Y., Agha-Amiri, K. & Klein, A. Selenium is involved in the negative regulation of the expression of selenium-free [NiFe] hydrogenases in *Methanococcus voltae*. *Mol. Gen. Genet.* **242**, 369–373 (1994).
29. Valente, F.M. *et al.* Selenium is involved in regulation of periplasmic hydrogenase gene expression in *Desulfovibrio vulgaris* Hildenborough. *J. Bacteriol.* **188**, 3228–3235 (2006).
30. Hatfield, D.L., Tsuji, P.A., Carlson, B.A. & Gladyshev, V.N. Selenium and selenocysteine: roles in cancer, health, and development. *Trends Biochem. Sci.* **39**, 112–120 (2014).
31. Reich, H.J. & Hondal, R.J. Why nature chose selenium. *ACS Chem. Biol.* **11**, 821–841 (2016).
32. Hondal, R.J., Marino, S.M. & Gladyshev, V.N. Selenocysteine in thiol/disulfide-like exchange reactions. *Antioxid. Redox Signal.* **18**, 1675–1689 (2013).
33. Hondal, R.J. & Ruggles, E.L. Differing views of the role of selenium in thioredoxin reductase. *Amino Acids* **41**, 73–89 (2011).
34. Snider, G.W., Ruggles, E., Khan, N. & Hondal, R.J. Selenocysteine confers resistance to inactivation by oxidation in thioredoxin reductase: comparison of selenium and sulfur enzymes. *Biochemistry* **52**, 5472–5481 (2013).
35. Reddie, K.G. & Carroll, K.S. Expanding the functional diversity of proteins through cysteine oxidation. *Curr. Opin. Chem. Biol.* **12**, 746–754 (2008).
36. Valente, F.M.A. *et al.* The [NiFeSe] hydrogenase from *Desulfovibrio vulgaris* Hildenborough is a bacterial lipoprotein lacking a typical lipoprotein signal peptide. *FEBS Lett.* **581**, 3341–3344 (2007).
37. Marques, M.C., Coelho, R., Pereira, I.A.C. & Matias, P.M. Redox state-dependent changes in the crystal structure of [NiFeSe] hydrogenase from *Desulfovibrio vulgaris* Hildenborough. *Int. J. Hydrogen Energy* **38**, 8664–8682 (2013).
38. Garcin, E. *et al.* The crystal structure of a reduced [NiFeSe] hydrogenase provides an image of the activated catalytic center. *Structure* **7**, 557–566 (1999).
39. Volbeda, A. *et al.* Structural foundations for the O_2 resistance of *Desulfomicrobium baculatum* [NiFeSe]-hydrogenase. *Chem. Commun. (Camb.)* **49**, 7061–7063 (2013).
40. Dementin, S. *et al.* A glutamate is the essential proton transfer gate during the catalytic cycle of the [NiFe] hydrogenase. *J. Biol. Chem.* **279**, 10508–10513 (2004).
41. Baltazar, C.S.A., Teixeira, V.H. & Soares, C.M. Structural features of [NiFeSe] and [NiFe] hydrogenases determining their different properties: a computational approach. *J. Biol. Inorg. Chem.* **17**, 543–555 (2012).
42. Lacasse, M.J. & Zamble, D.B. [NiFe]-hydrogenase maturation. *Biochemistry* **55**, 1689–1701 (2016).
43. Watanabe, S. *et al.* Structural basis of a Ni acquisition cycle for [NiFe] hydrogenase by Ni-metallochaperone HypA and its enhancer. *Proc. Natl. Acad. Sci. USA* **112**, 7701–7706 (2015).
44. Gutiérrez-Sanz, O. *et al.* Influence of the protein structure surrounding the active site on the catalytic activity of [NiFeSe] hydrogenases. *J. Biol. Inorg. Chem.* **18**, 419–427 (2013).
45. Leinfelder, W., Zehelein, E., Mandrand-Berthelot, M.A. & Böck, A. Gene for a novel tRNA species that accepts L-serine and cotranslationally inserts selenocysteine. *Nature* **331**, 723–725 (1988).
46. Zhang, Y., Romero, H., Salinas, G. & Gladyshev, V.N. Dynamic evolution of selenocysteine utilization in bacteria: a balance between selenoprotein loss and evolution of selenocysteine from redox active cysteine residues. *Genome Biol.* **7**, R94 (2006).
47. Ogata, H., Nishikawa, K. & Lubitz, W. Hydrogens detected by subatomic resolution protein crystallography in a [NiFe] hydrogenase. *Nature* **520**, 571–574 (2015).

Acknowledgments

We thank F. Grein and M. Martins for advice and helpful discussions, R. Coelho and S. Silva for help with crystallization procedures and S. Zacarias for experimental assistance; ESRF, DLS and SOLEIL light sources for X-ray data collection; V. Olieric (Swiss Light Source) for the 0.95-Å data collection of the anaerobically purified and crystallized r[NiFeSe] hydrogenase. This work was supported by grants PTDC/BBB-BEP/0934/2012 and PTDC/BBB-BEP/2885/2014 (to I.A.C.P. and P.M.M.) from the Fundação para a Ciência e Tecnologia (FCT/MCTES), by research units GREEN-IT (UID/Multi/04551/2013) funded by FCT/MCTES, and MOSTMICRO (project LISBOA-01-0145-FEDER-007660) co-funded by FCT/MCTES and FEDER funds through COMPETE2020—Programa Operacional Competitividade e Internacionalização (POCI); and by Spanish MINECO/FEDER project CTQ2015-71290-R (to A.L.D.L.). M.C.M. was a recipient of fellowship SFRH/BD/60879/2009 and C.T. was a recipient of predoctoral contract BES-2013-064099 from MINECO. This work was also supported by the European Community's Seventh Framework Program (FP7/2007–2013) under grant agreement 283570 (BioStruct-X).

Author contributions

I.A.C.P., P.M.M. and M.C.M. conceived the study. A.R.R., K.L.K., J.D.W. and M.C.M. carried out the molecular biology work. M.C.M. and I.A.C.P. produced and characterized hydrogenase variants. M.C.M. and P.M.M. were involved in crystallization and structure determination. O.G.-S., C.T. and A.L.D.L. carried out FTIR and MS experiments. I.A.C.P., P.M.M. and M.C.M. wrote the manuscript with input from other authors.

Competing financial interests

The authors declare no competing financial interests.

Additional information

Any supplementary information, chemical compound information and source data are available in the online version of the paper. Reprints and permissions information is available online at http://www.nature.com/reprints/index.html. Correspondence and requests for materials should be addressed to X.X.

ONLINE METHODS

Genetic constructs. A mutant strain lacking the *hysA* and *hysB* genes (below referred to as *hysAB*) encoding the [NiFeSe] hydrogenase was produced by double homologous recombination in *D. vulgaris* as described[48], generating strain IPAR01 (electroporation parameters: 1.500 V, 250 Ω, and 25 μF). For the *hysAB* deletion, the plasmid pMOIP01 was produced by sequence ligation independent cloning (SLIC)[49]. Three segments were amplified by PCR: 1,055 bp upstream of *hysAB* (*hysAB* Up Fw – GCCTTT TGCTGGCCTTTTGCTCACATGGACAAGG ATGAGCCCGTTGTGA A and *hysAB* Up Rev – AAGACTGTAGCCGTACCTCGAATCTATG C AGTGCCAGCCAATAGAGTGAA), 885 bp downstream of *hysAB* (HysAB Dwn Fw –AAT CCGCTCACTAAGTTCATAGACCGGACGCCCAT GATGTTAGGGTTCCAA and *hysAB* Dwn Rev – CGAGGCATTTCTG TCCTGGCTGGGCGTACGCATTACGCA CGTATCAT) and the kanamycin resistance gene from pSC27[48] (Kan 1Fw–TAGATTCGAGGT ACGGCTACAGTCTTACGGTCACAAACAGGTACGCCCCCAGAGTC and Kan 2 Rev –CGGTCTATGAACTTAGTGAGCGGATTTCTCGTGT AGCCGATGCAGTGAGGTAGCTTGCAG); and then added to the pMO719 background via SLIC. The products from the amplifications were transformed into *E. coli* α-select Silver Efficiency (Bioline), and successful transformants were isolated on LB medium containing 50 μg/ml kanamycin and 100 μg/ml spectinomycin. Correct isolates were identified by the expected PCR amplicons from the plasmid constructs and also by sequencing performed at the DNA Core Facility at the University of Missouri. The pMOIP01 plasmid was electroporated into *D. vulgaris* according to a previous established protocol[48], from which strain IPAR01 (Δ*hys*AB) was obtained, by selecting with MOYLS4 medium containing 400 μg/ml geneticin. The deletion of *hysAB* was confirmed by Southern blot using as probe an upstream fragment of the *hysAB* genes.

To produce the soluble form of HysAB, an expression vector was constructed encoding the *hysB* gene followed by a *Strep*-tag and the *hysA* gene lacking the first 11 amino acid residues. To create this vector, two segments were amplified by PCR: the *hysB* gene (HysB Exp Vctr Fw – AGGTTGGGAAGCCCTGCAATG CAGTCCCAGGAGGTACCATATGAGTCTCACAAGGCGTGATTTCGTC and HysB Exp Vctr Rev –TTTTTCGAACTGCGGGTGGCTCCACATGATAT CCTCCTGAAGCGACTGACGG) and the *Strep*-tag with the *hysA* gene (HysA Exp Vctr Fw - TGGAGCCACCCGCAGTTCGAAAAA GGGGCCACC GGCAGGACGACCATC and HysA Exp Vctr Rev– GATCGTGATCCCCTGCGC CATCAGATCCTTGGCTCGCGGCCCCTCCCCTTCATGAT); and then added into pMO9075 background via SLIC. The amplification products were transformed into *E. coli* α-select Silver Efficiency, and cells were plated on spectinomycin (100 μg/ml)-containing agar plates. The correct plasmid construct was screened by colony PCR and later confirmed by sequencing at the DNA Core Facility at the University of Missouri. The pMOIP03 vector was successfully introduced in IPAR01 by electroporation[48] in MOYLS4 medium containing 400 μg/ml geneticin and 100 μg/ml spectinomycin, generating the complemented strain IPMM01. The plasmid was confirmed by PCR amplification of the insert and also by sequencing performed at GATC Biotech.

The amino acid exchange Sec489Cys in the large subunit (HysA) of the *D. vulgaris* [NiFeSe] hydrogenase was generated by the NZYMutagenesis kit using the mutagenic primers 5′-TGCACGGCACAGCCCAGGCACGG GTCGAAGGCGCG-3′ and 5′-CGCGCCTTCGACCCG TGCCTGGGCTGT GCCGTGCA-3′. Plasmid pMOIP03 carrying a $hysA_{Strep}hysB$ fragment was used as the template. The amplification products were transformed into *E. coli* α-select Silver Efficiency and the new plasmid construct named pMOIPM02 was screened by colony PCR and sequencing at GATC Biotech. The pMOIPM02 vector was used for homologous recombination using strain IPAR01, generating the complemented strain IPMM02.

Cell growth and protein purification. All *D. vulgaris* strains were cultivated in modified Postgate medium C with an iron concentration of 25 μM. This medium has lactate as electron donor and sulfate as electron acceptor, and nickel chloride and sodium selenide, both at a concentration of 1 μM, unless otherwise stated. The cells synthetizing the r[NiFeSe] hydrogenase (IPMM01) were harvested at late exponential phase, resuspended in 20 mM Tris-HCl buffer, pH 7.6, and disrupted in a French pressure cell, under a N_2 atmosphere to prevent O_2 exposure. The soluble fraction was obtained by ultracentrifugation (42,000 × *g*, 90 min). Purification was carried out both under aerobic and anaerobic conditions. Anaerobic purifications were carried out inside a Coy anaerobic chamber (95% N_2, 5% H_2) using an AKTA Prime plus system. The soluble fraction was applied to a Q-Sepharose HP column equilibrated with 20 mM Tris-HCl, pH 7.6, buffer. A stepwise NaCl gradient was performed and fractions were separated according to their UV–visible spectra. The fractions containing hydrogenase, which eluted between 200 and 300 mM NaCl, were pooled. The buffer was exchanged to 20 mM Tris-HCl, pH 8.0, by concentrating the fractions with a 30-kDa cutoff ultracentrifugation unit (Amicon Ultra-15 30K NMWL, Millipore) and then loaded onto a column containing Strep-Tactin resin (IBA GmBH) equilibrated with 50 mM Tris-HCl, pH 8.0, 150 mM NaCl (Buffer W). After five washing steps with Buffer W, the recombinant protein was eluted with eluting buffer (Buffer W + 2.5 mM desthiobiotin). Protein concentration was determined with the bicinchoninic acid assay from Pierce using BSA as standard.

***In vitro* metal reconstitution of the Sec489Cys hydrogenase.** For *in vitro* nickel reconstitution of the Sec489Cys hydrogenase, 1 or 5 mM $NiCl_2 \cdot 5H_2O$ was present in the buffer for disruption of IPMM02 cells. After purification, 100 μl of the nickel-depleted protein at 100 μM was incubated under anaerobic conditions with 100 μl 20 mM Tris-HCl buffer at pH 8.0 containing 0, 1 or 5 mM $NiCl_2 \cdot H_2O$, at room temperature (RT) for 1 h, under a H_2 atmosphere. The protein was subsequently washed several times with 20 mM Tris-HCl, pH 7.6, buffer, and concentrated, using Amicon Ultra centrifugal filters 30K for the crystallization trials and pH activity profiles. For the ICP, FTIR and EPR experiments, the Sec489Cys hydrogenase eluted from the affinity column was washed five times with 20 mM Tris-HCl, pH 7.6, buffer with 5 mM $NiCl_2 \cdot H_2O$ using Amicon Ultra centrifugal filters 30K, to remove traces of desthiobiotin. The protein was subsequently incubated at RT under H_2 with 20 mM Tris-HCl, pH 7.6, and 5 mM $NiCl_2 \cdot H_2O$ for 1 h. After the incubation, the reconstituted enzyme was washed five times with 20 mM Tris-HCl, pH 7.0, 1 mM EDTA and concentrated with a 30-kDa cutoff ultracentrifugation unit (Amicon Ultra-15 30K).

Western blot analysis. The crude cell extracts were run on a 12% SDS–PAGE gel. Proteins were then transferred to 0.45-μm polyvinylidene difluoride membranes (Roche) for 1 h at 100 mV and 4 °C in a Mini Trans-Blot Electrophoretic Transfer Cell (Bio-Rad). The membranes were equilibrated with Tris-buffered saline solution with Tween-20 (TBST; 20 mM Tris-HCl, pH 7.5, 150 mM NaCl, 0.05% Tween-20), and then treated with antiserum raised against the native *D. vulgaris* [NiFeSe] hydrogenase[29]. The antibody was diluted 1:500 in TBST. Immunodetection was performed by treatment with anti-mouse immunoglobulin G (heavy plus light chain) alkaline phosphatase conjugate (from Sigma) diluted 1:5,000, followed by a solution of nitroblue tetrazolium salt and 5-bromo-4-chloro-3-indolyl phosphate toluidine salt (NBT/BCIP solution; Roche).

H_2 production by gas chromatography. Hydrogenase activity was routinely assayed by H_2 production as previously described[13], unless otherwise stated. The activity of the crystallized protein was measured immediately after dissolving crystals harvested from the crystallization drop in 50 μl 20 mM Tris-HCl, pH 7.6, buffer.

Hydrogenase uptake activity assays. The H_2 uptake activities of r[NiFeSe] and Sec489Cys hydrogenases were measured spectrophotometrically in a Coy anaerobic chamber (95% N_2, 5% H_2) with methyl viologen (MV) as the electron acceptor, as previously described[50]. The purified enzyme was activated for approximately 1 h at RT in an anaerobic vial containing 1 mL of 50 mM Tris-HCl buffer at pH 7.0 with 1 mM MV and traces of dithionite. H_2 oxidation activity was measured at 37 °C in a cuvette containing 1 mL 50 mM Tris-HCl buffer, pH 7.0, and 2 mM MV with a trace of dithionite to eliminate residual oxygen. The sample vials and buffers were saturated with pure H_2 after oxygen removal under vacuum. The reaction was started by the addition of 10 μL stock solution of activated r[NiFeSe] hydrogenase (5–10 μM range) and Sec489Cys hydrogenase (50–100 μM range), and the rate of MV reduction was measured at 604 nm, with a UV–VIS spectrophotometer (Shimadzu). Specific

doi:10.1038/nchembio.2335

activities were determined in a range of concentrations where linearity of activity with protein concentration was established. Each enzyme assay was carried out in triplicate. For the pH dependency assays, a buffer mix was used containing sodium citrate, MES, HEPES, Tris and sodium carbonate, each at 10 mM concentration. Activity-stained native-PAGE was performed as previously described[13].

Hydrogen–deuterium exchange activity. The D_2–H^+ exchange activity of *D. vulgaris* hydrogenases was measured by membrane-inlet mass spectrometry, in which a thermostatized anaerobic vessel at 37 °C with magnetic stirring was connected through a 14-µm Teflon membrane to a mass spectrometer (Pfeiffer Prisma). The output signal of the spectrometer for each mass value is proportional to the partial pressure of the corresponding gas in the reaction vessel. The output signal was first calibrated by saturating the reactor solution with 100% H_2 and then by 20% D_2 in 80% Ar (Air Liquide). The D_2–H^+ assays were performed as previously described[44] in a buffer mix containing sodium citrate, MES, HEPES, Tris and sodium carbonate, each at 10 mM concentration.

FTIR spectroscopy. Hydrogenase samples in Tris-HCl buffer (pH 7.6) were first concentrated to 100 µM by ultrafiltration for measurements in a transmission CaF_2 cell with 82-µm path length. The FTIR spectra were recorded at 2-cm^{-1} resolution and averaging 1,024 scans using a Bruker Tensor 27 Fourier transform spectrometer, equipped with a mercury cadmium telluride detector and a purge gas system (Whatman) for removal of CO_2 and H_2O. A transmission cell with CaF_2 windows was used for standard FTIR measurements.

Circular dichroism spectroscopy. CD measurements were carried out in a JASCO spectropolarimeter J-810, using cuvettes of 1.0-mm path length. Spectra were acquired at 20 °C between 195 and 260 nm, with data pitch of 0.5 nm, wavelength sampling velocity of 100 nm min^{-1} and performing at least five accumulations. All spectra were normalized to mean residue molar ellipticity (deg cm^2 $dmol^{-1}$ res^{-1}).

Electron paramagnetic resonance spectroscopy. EPR spectra were obtained using a Bruker EMX spectrometer equipped with an ESR-900 continuous flow helium cryostat. Measurements were performed at pH 7.6. The EPR conditions were T = 90 K, microwave power 2.013 mW; modulation amplitude 1 mT and microwave frequency 9.508 GHz.

Crystallization and X-ray diffraction data collection. Crystals of the aerobically purified r[NiFeSe] hydrogenase (r[NiFeSe]-Ox) and Sec489Cys hydrogenase (Sec489Cys-Ox) were obtained aerobically at room temperature by the sitting drop vapor diffusion method, using 20% PEG 1500 (w/v) and 0.1 mM Tris-HCl (pH 7.6) as precipitant. The protein concentrations used were 9.2 and 12.5 mg/mL, respectively. Crystallization drops were prepared by mixing 1 µL protein solution with an equal volume of precipitant and equilibrated against 500 µL reservoir. For the Ni-reconstituted Ni-Sec489Cys-Ox hydrogenase crystals, a 12 mg/mL protein solution and 20% PEG 3350 and 0.2 M sodium malonate as precipitant were used. The crystals appeared after 1 week, were cryoprotected using a solution containing 20% glycerol, 20% PEG 1500 (w/v) and 0.1 mM Tris-HCl (pH 7.6) (r[NiFeSe]-Ox and Sec489Cys-Ox) and 20% glycerol, 20% PEG 3350 and 0.2 M sodium malonate (Ni-Sec489Cys-Ox), flash-cooled in N_2 (liquid) and stored. Diffraction data from the r[NiFeSe]-Ox, Sec489Cys-Ox and Ni-Sec489Cys-Ox crystals were collected at the European Synchrotron Radiation Facility (ESRF) in Grenoble, France. Data from the r[NiFeSe]-Ox crystal were collected at beamline ID14-1 on an ADSC Q210 detector using a wavelength of 0.9334 Å; data from the Sec489Cys-Ox crystal were collected at beamline ID14-4 on an ADSC Q315r detector using a wavelength of 0.9701 Å; and data from the Ni-Sec489Cys-Ox crystal were collected at beamline ID23-2 on a PILATUS3 2M detector using a wavelength of 0.8726 Å. A preliminary Ni-Sec489Cys-Ox data set was also collected at beamline PROXIMA II of the SOLEIL synchrotron in St. Aubin, France.

The anaerobic crystallization drops for the anaerobically purified r[NiFeSe] hydrogenase and reconstituted Ni-Sec489Cys hydrogenase Ni-Sec489Cys were first prepared inside a Coy anaerobic chamber (95% N2, 5% H_2), and then placed inside an anaerobic Genbox (Biomerieux). The protein concentrations used were 10.4 and 15.5 mg/mL respectively. Crystallization drops were prepared by mixing 2 µL protein solution with an equal volume of precipitant (20% PEG 1500 (w/v) and 0.1 mM Tris-HCl, pH 7.6) and equilibrated against 500 µL reservoir. Crystals of r[NiFeSe] and Ni-Sec489Cys appeared after 1 week and were cryoprotected using a solution containing 20% glycerol, 20% PEG 1500 (w/v) and 0.1 mM Tris-HCl, pH 7.6. The crystals were quickly harvested in a plastic glove box flushed with N_2 (gas), flash-cooled in N_2 (liquid) and stored. Diffraction data from the r[NiFeSe] were collected at the PXIII beamline of the Swiss Light Source (SLS) at the Paul Scherrer Institute in Villigen, Switzerland using a PILATUS 2M-F detector and a wavelength of 0.7514 Å; data from the Ni-Sec489Cys crystal were measured at the I02 beamline of the Diamond Light Source (DLS) in Didcot, UK, using a PILATUS 6M-F detector and a wavelength of 0.9795 Å. All data sets were collected at 100 K, and the wavelength chosen was on the high-energy side of the K-absorption edge of the selenium atom. The diffraction images were indexed and integrated using XDS[51], and conversion of intensities to structure factor amplitudes was carried out with CTRUNCATE in the CCP4 program suite[52]. The data collection and processing statistics are listed in **Supplementary Table 2**.

Structure determination and refinement. The crystal structures were determined by the molecular replacement method with PHASER[53] via the CCP4 Graphics User Interface[54]. The coordinates of the protein chains of the large and small subunits of the previously published crystal structure of *D. vulgaris* [NiFeSe] hydrogenase (PDB 2WPN)[20] were used as search models, after removal of all non-protein atoms. Following a quick initial refinement with REFMAC[55], COOT[56] was used to perform model corrections and addition of the active site metals and Fe–S clusters. Refinement was continued with PHENIX[57], consisting of 3–5 macrocycles with refinement of positional coordinates, individual isotropic atomic displacement parameters for all non-hydrogen atoms (and also refinement of the anomalous dispersion parameters for the Se atom, in the case of the r[NiFeSe] and r[NiFeSe]-Ox structures. Model inspection and editing was done with COOT[56] against σ_A-weighted $2|F_o| - |F_c|$ and $|F_o| - |F_c|$ electron density maps. Water molecules were added with PHENIX and checked with COOT. Hydrogen atoms in calculated positions were added to the structural models and included in the refinement in riding positions. In the final refinement stages, individual anisotropic atomic displacement parameters for all protein non-hydrogen atoms were refined for all structures.

In the crystal structure of the anaerobically purified and crystallized r[NiFeSe] hydrogenase, the occupancy factors of the two Ni sites were refined independently, allowing for incomplete Ni incorporation into the active site. The sum of the occupancy factors of the three selenocysteine positions was constrained to unity. A positive feature in the final $|F_o| - |F_c|$ map (**Fig. 1c**) could be due to a different minor Fe conformation (not modeled).

In the crystal structure of the as-isolated Sec489Cys hydrogenase (Sec489Cys-Ox), the sum of the occupancy factors of the Ni and S sites and of the three forms of Cys75 were constrained to unity. The probable predominant structural forms of the active site and their relative percentages (**Fig. 2b**,**c**) were interpreted from the final refined structure: the first is estimated from the refined occupancy of the Ni site and the second from the combined occupancies of the non-oxidized Cys75 conformers forming a disulfide bridge with Cys78. The percentages do not add up to 100% because we could not uniquely identify the remaining structural forms.

In the crystal structure of the anaerobically purified and crystallized Ni-Sec489Cys hydrogenase, the occupancy factors of the three Ni sites and the exogenous sulfur atom were refined independently. The probable predominant structural forms of the active site and their relative percentages (**Fig. 3b–d**) were interpreted from the final refined structure.

MOLPROBITY[58] was used to investigate model geometry in combination with the validation tools provided in COOT. For all the five crystal structures reported here, the number of Ramachandran outliers did not exceed 0.13% of the total number of non-proline and non-glycine residues, and the MOLPROBITY clash score did not exceed 2.0. The refinement statistics are included in **Supplementary Table 2**. Figures were generated using the PyMOL Molecular Graphics System, Version 1.7.1 (Schrödinger, LLC).

Data availability. The final atomic coordinates and experimental structure factors were deposited in the Worldwide Protein Data Bank with accession codes 5JSH, 5JSK, 5JSU, 5JSY and 5JT1 for the r[NiFeSe]-Ox, r[NiFeSe], Sec489Cys-Ox, Ni-Sec489Cys and Ni-Sec489Cys-Ox structures, respectively. All other data supporting the findings of this study are available within the paper and its supplementary information files.

48. Keller, K.L., Wall, J.D. & Chhabra, S. Methods for engineering sulfate reducing bacteria of the genus *Desulfovibrio*. *Methods Enzymol.* **497**, 503–517 (2011).
49. Li, M.Z. & Elledge, S.J.S.L.I.C. SLIC: a method for sequence- and ligation-independent cloning. *Methods Mol. Biol.* **852**, 51–59 (2012).
50. Dementin, S. *et al.* Changing the ligation of the distal [4Fe4S] cluster in NiFe hydrogenase impairs inter- and intramolecular electron transfers. *J. Am. Chem. Soc.* **128**, 5209–5218 (2006).
51. Kabsch, W. Automatic processing of rotation diffraction data from crystals of initially unknown symmetry and cell constants. *J. Appl. Crystallogr.* **26**, 795–800 (1993).
52. Winn, M.D. *et al.* Overview of the CCP4 suite and current developments. *Acta Crystallogr. D Biol. Crystallogr.* **67**, 235–242 (2011).
53. McCoy, A.J. Solving structures of protein complexes by molecular replacement with Phaser. *Acta Crystallogr. D Biol. Crystallogr.* **63**, 32–41 (2007).
54. Potterton, E., Briggs, P., Turkenburg, M. & Dodson, E. A graphical user interface to the CCP4 program suite. *Acta Crystallogr. D Biol. Crystallogr.* **59**, 1131–1137 (2003).
55. Murshudov, G.N., Vagin, A.A. & Dodson, E.J. Refinement of macromolecular structures by the maximum-likelihood method. *Acta Crystallogr. D Biol. Crystallogr.* **53**, 240–255 (1997).
56. Emsley, P., Lohkamp, B., Scott, W.G. & Cowtan, K. Features and development of COOT. *Acta Crystallogr. D Biol. Crystallogr.* **66**, 486–501 (2010).
57. Adams, P.D. *et al.* PHENIX: a comprehensive Python-based system for macromolecular structure solution. *Acta Crystallogr. D Biol. Crystallogr.* **66**, 213–221 (2010).
58. Chen, V.B. *et al.* MolProbity: all-atom structure validation for macromolecular crystallography. *Acta Crystallogr. D Biol. Crystallogr.* **66**, 12–21 (2010).

doi:10.1038/nchembio.2335